



**HAL**  
open science

# Detection of kissing bond type defects and evaluation of the bonding quality in metal/adhesive/composite structures by a wavenumber-frequency insensitive SH mode

Latifa Attar, Mounsif Ech Cherif El Kettani, Damien Leduc, Mihai Valentin Predoi, Jocelyne Galy

## ► To cite this version:

Latifa Attar, Mounsif Ech Cherif El Kettani, Damien Leduc, Mihai Valentin Predoi, Jocelyne Galy. Detection of kissing bond type defects and evaluation of the bonding quality in metal/adhesive/composite structures by a wavenumber-frequency insensitive SH mode. *NDT & E International*, 2023, 137, pp.102841. 10.1016/j.ndteint.2023.102841 . hal-04073283

**HAL Id: hal-04073283**

**<https://hal.science/hal-04073283>**

Submitted on 18 Apr 2023

**HAL** is a multi-disciplinary open access archive for the deposit and dissemination of scientific research documents, whether they are published or not. The documents may come from teaching and research institutions in France or abroad, or from public or private research centers.

L'archive ouverte pluridisciplinaire **HAL**, est destinée au dépôt et à la diffusion de documents scientifiques de niveau recherche, publiés ou non, émanant des établissements d'enseignement et de recherche français ou étrangers, des laboratoires publics ou privés.

# Detection of kissing bond type defects and evaluation of the bonding quality in metal/adhesive/composite structures by a wavenumber-frequency insensitive SH mode

Latifa Attar<sup>a</sup>, Mounsif Ech Cherif El Kettani<sup>a</sup>, Damien Leduc<sup>a,\*</sup>, Mihai Valentin Predoi<sup>b</sup>,  
Jocelyne Galy<sup>c</sup>

<sup>a</sup> *Laboratoire Ondes et Milieux Complexes (LOMC), UMR CNRS 6294, University Le Havre Normandy, 75 rue Bellot, 76600 Le Havre, France*

<sup>b</sup> *Department of Mechanics, University Politehnica of Bucharest, Splaiul Independentei, 313, sect. 6, Bucharest, 060042 Bucharest, Romania*

<sup>c</sup> *Laboratoire Ingénierie des Matériaux Polymères (IMP), UMR CNRS 5223, INSA Lyon, Bâtiment Jules Verne 17, avenue Jean Capelle, 69621 Villeurbanne, France*

\* Corresponding author.

E-mail address: [damien.leduc@univ-lehavre.fr](mailto:damien.leduc@univ-lehavre.fr) (D. Leduc).

## **Abstract**

This work focuses on the non-destructive evaluation of the bonding quality in different metal/adhesive/composite samples and on the detection of defects simulating a kissing bond, using Shear Horizontal (SH) guided waves. A predictive 2D numerical model, called interphases model and based on finite elements method describing the interface substrate/adhesive by a very thin layer, is developed. Various samples with different adhesion levels obtained by modifying the cohesive and adhesive aspects or including a defect representing a kissing bond are investigated. An experimental study is performed with non-contact ElectroMagnetic Acoustic Transducers (EMAT) in excitation and reception. As the wavenumber-frequency sensitive SH modes to the adhesion quality shown by the numerical predictions are not easy to generate experimentally, the analysis of the behaviour of the SH modes is based here on their amplitude. Results show that it is possible to differentiate between the adhesion levels due to different epoxy conversion, the presence or absence of an adhesion promoter or a pollution by a release agent, as well as the detection of the defect.

**Keywords:** ultrasonic bond testing; ultrasonic guided waves; shear horizontal waves; EMAT; composite material; non-destructive evaluation; kissing bond defect.

## 1. Introduction

Bonded structures are extensively used in various industrial applications. They are particularly common throughout the aeronautical and automotive industries [1]. They have many advantages over conventional techniques (bolting, riveting) such as weight reduction, better mechanical stress distribution across the bonded area and ease of manufacture. One of the limitations of adhesive joints is the difficulty in predicting the joint strength throughout their live cycle, due to the possible presence of defects in the adhesive e.g. holes, weak bonding, local dis-bonding, kissing bond...[2–4]. The control of the quality of the bonding is therefore of utmost interest. For example, Federal Aviation Administration (F.A.A, U.S.A) circular AC20-107B for the certification of composite structures notes that many of the qualification problems of new aircraft are related to the failure to qualify bonded structures. So, current aviation regulations still require the use of traditional fasteners in the absence of reliable control of the glued assemblies.

The use of ultrasonic waves to non-destructively inspect the adhesive bonding strength has become one of the most extensively applied technologies [5]. Many works have been reported on the general topic of ultrasonic non-destructive evaluation (NDE) of adhesive bonds, using mainly either Lamb or Shear-Horizontal (SH) guided waves [6–9] as they are found to be efficient to characterize adhesive bond properties [10–13]. In this work, we present an evaluation of the bonding quality using SH ultrasonic guided waves. The generation and detection of these waves is achieved using electromagnetic acoustic transducers (EMAT). EMATs are non-contact sensors that do not require the use of a coupling gel and have been shown to be effective on rough and corroded surfaces [14]: they simplify measurements and comparisons due to their reproducibility.

In this present paper, we are interested in the propagation of SH waves in metal/epoxy adhesive/carbon-epoxy assemblies, with different surface treatments applied on the substrate,

and different cure levels of the epoxy which affects the quality and strength of the bonding. The amplitude measurements of the propagating SH wave enable to discriminate the different samples and to detect the presence of a kissing bond type defect and its signature. In fact, previous work [15] has shown that the use of the dispersion curves as indicator for the quality of the bonding is not efficient, as the SH modes sensitive to the interfacial strength substrate-adhesive cannot be generated. Consequently, the signal treatment in this work is focused on the amplitude variations of the propagating SH wave. Experimentally, Flynn [16] and C. Gauthier et al [17–19] showed that the attenuation coefficient of guided waves in the medium were indeed related to the bonding strength and stiffness of the adhesives. In the field of non-destructive evaluation by SH type guided waves, mostly modes SH<sub>0</sub>, SH<sub>1</sub> and rarely SH<sub>2</sub> or SH<sub>3</sub> have been exploited [20–23], aiming to identify defects of cohesive or adhesive nature or to detect the adhesive layer thickness [23]. In the present study, a higher order SH<sub>3</sub> mode has been used, based on the propagation properties of this mode in the different samples. The amplitude variations of this mode during its propagation should give information about the quality of the bonding and the presence of a defect and its location. After describing the characteristics of the samples studied in section 2, a predictive 2D numerical model, based on finite elements method and representing the interface substrate/adhesive by a very thin layer, called interphase, is established and solved in section 3. The result of the numerical approach using a finite element model to predict the behaviour of the given SH mode within the three-layer structure with different interfacial and cohesive bonding conditions are then compared with experimental measurements. A quantitative study of the attenuation of the SH<sub>3</sub> mode is carried out in section 4 and it is shown that the attenuation of this mode is a good criterion for detecting and locating a kissing bond defect and for assessing different adhesion levels.

## 2. Description of the samples

Three samples of three-layer aluminium/adhesive/carbon-epoxy composite were made for this study. Each of them is made of different substrates of aluminium and composite 300 mm long and 200 mm wide. The structural adhesive used for assembling is a two-component epoxy adhesive formula. It consists of a resin, called DGEBA (Diglycidyl Bisphenol Ether A), manufactured by Huntsman with the reference LY 556 and in stoichiometric proportion to a hardener, Jeffamine D 230, which is an aliphatic diamine manufactured also by Huntsman [17]. The thickness of the substrates are respectively 4 mm and 1.8 mm for the aluminium plate and the composite, whereas the adhesive has a thickness of 0.5 mm.

The first assembly is made by degreasing aluminium with isopropanol to remove all the impurities and applying a chemical treatment with Silane which is an adhesion promoter. It highly improves the level of adhesion between the aluminium and the adhesive by creating strong chemical bonds (covalent bonds). On the composite side, the plate was directly glued after tearing the protective film. Tearing off this film creates a certain surface roughness of less than 15  $\mu\text{m}$  on the interface to be glued, which improves the level of adhesion of this sample. The cross-linking rate of the epoxy adhesive is 100%. To reach this crosslinking level, the assembly is placed in a press for 1 hour at 80 °C and then 3 hours at 160 °C [17]. This sample is noted  $Al_{DSi}E_{100}C_N$ : DSi for degreasing and silanization; N for normal i.e. no special treatment on the composite/adhesive interface. This sample is considered in the following as the reference sample with the highest level of adhesion.

The second sample underwent a simple degreasing on the aluminium/adhesive interface. Once the assembly was completed, it was left in press for 48 hours at room temperature. The cross-linking rate of the adhesive is then 80% [17]. As for the first sample, no particular treatment was done on the composite/adhesive interface. This sample is noted  $Al_D E_{80} C_N$  and

has an expected intermediate level of adhesion on the aluminium side and a high adhesion on the composite side.

A third sample is chemically treated with silane at the aluminium/adhesive interface on one side and a release agent layer has been deposited on the other side. A good adhesion is expected on the non-polluted area and a lack of adhesion on the other side. The length of each area is the half of the total length of the guide. The composite/adhesive interface has not undergone any treatment and the adhesive was 100% crosslinked. This sample will be called  $Al_{1/2DSi-1/2DRA}E_{100}C_N$ . The studied samples are listed in Table 1.

Nomenclature	Aluminum treatment surface	Composite treatment surface	Epoxy crosslinking rate
$Al_{DSi}E_{100}C_N$ (Reference)	Degreased and silanized	Normal	100%
$Al_DE_{80}C_N$	Only degreased	Normal	80%
$Al_{\frac{1}{2}DSi\frac{1}{2}DRA}E_{100}C_N$	One half: degreased and silanized Second half: degreased and release agent	Normal	100%

**Table 1.** Studied three-layer assemblies and associated nomenclature.

### 3. Detection of a kissing-bond type defect

#### 3.1 Predictive numerical study using a 2D interphases model

The objective of this 2D model is to predict the behaviour of a guided SH mode when crossing a kissing bond defect. We will look for the evolution of the amplitude of a given SH mode versus the distance and will compare with the experimental results.

The modelled three-layer is shown in Fig. 1. Each layer (aluminium, composite and adhesive) is characterized by its thickness (respectively  $h_A, h_C$  and  $d$ ), its density ( $\rho_A, \rho_C$  and  $\rho_E$ ) and the modulus of elasticity  $C_{44}$  and  $C_{55}$  for each layer. These parameters are given in Table 2.

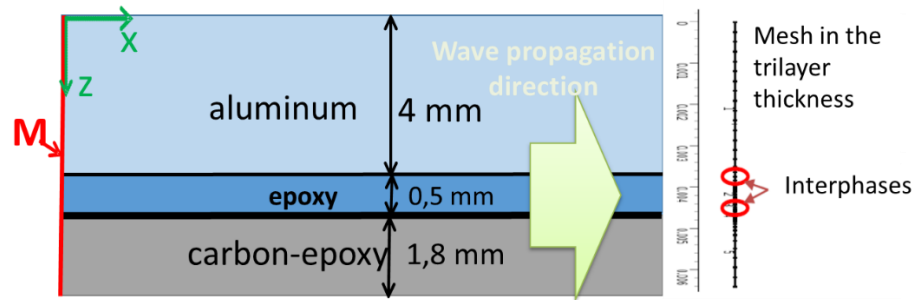


**Fig. 1.** Geometry of the three-layer aluminium/epoxy/carbon-epoxy. Mesh used in the SAFE method for the dispersion curves (right).

Material	$\rho$ (kg/m <sup>3</sup> )	$C_{44}$ (GPa)	$C_{55}$ (GPa)	Thickness (mm)
Aluminium	2800	26.91	26.91	4
Epoxy	1160	1.46	1.46	0.5
Carbon-epoxy composite	1700	4.87	4.87	1.8

**Table 2.** Materials properties.

### 3.1.1 Description of the numerical model

The aim is to develop a numerical model based on finite elements, for the propagation of SH waves in a metal/adhesive/composite structure. A 2D temporal model to simulate the propagation of a given SH mode, similar to the experimental study, was developed with the

finite element software Comsol Multiphysics [24]. This model allows comparisons with experimental measurements using similar signal processing. This involves modelling the three-layer in the plane  $(x_1, x_3)$  of its section (see Fig. 1). The link between the substrate and the adhesive is modelized by a thin layer called interphase [25]. The formation of an interphase is governed by interactions and chemical reactions between the substrate and the adhesive. These interactions are then different from one association substrate-adhesive to another which makes the interphase specific to each association, and then can be indicator on the quality of the bonding. The physico-chemical properties of these interphases depend on the nature of the substrate and the adhesive [26]. In the case of perfect adhesion, each elastic constant of the interphase was defined as the average value between that of the substrate and that of the adhesive. For the various levels of adhesion, this averaged value is weighted by a coefficient  $\alpha$  for the aluminium/adhesive interphase and  $\beta$  for the carbon-epoxy/adhesive one. These coefficients vary from 0 (in the case of the delamination) to 1 (in the case of a perfect adhesion) for each interphase, such as [26]:

$$\begin{cases} C_{44} = C_{55} = \alpha \left( \frac{C_{55}^{epoxy} + C_{55}^{aluminium}}{2} \right) \\ C'_{44} = C'_{55} = \beta \left( \frac{C_{55}^{epoxy} + C_{55}^{carbon-epoxy}}{2} \right) \end{cases} \quad (1)$$

The modulus of elasticity  $C_{44} = C_{55}$  are related to the aluminium/adhesive interphase and  $C'_{44} = C'_{55}$  for the adhesive/carbon-epoxy interphase.

As the coupling between the substrate and the adhesive is linked to the penetration of the adhesive in the roughness of the substrate (wettability), the thickness of the interphases is taken as to the natural roughness of the substrates [25]. Surface profile measurements are made on each of the aluminium and composite plates using a Surface Roughness Measuring Instrument (Mitutoyo SV-1200). The measurement of the root mean square deviation of the

profile (called  $R_q$ ), the thickness of the aluminium/adhesive and composite/adhesive interphases can therefore be estimated. The results are given in Table 3. The thickness of the interphase is deducted from the thickness of the substrate concerned so that the total thickness of the structure remains unchanged.

Interphase	$C_{44}$ (GPa)	$C_{55}$ (GPa)	Thickness (mm)
Aluminum/epoxy interphase	14.18	14.18	$1.00 \cdot 10^{-3}$
Epoxy/carbon-epoxy interphase	3.16	3.16	$15.0 \cdot 10^{-3}$

**Table 3.** Interphases properties.

To model the displacement of SH waves in the studied structure, the following differential equation is used in Comsol Multiphysics [24]:

$$e_a \frac{\partial^2 w}{\partial t^2} + \nabla \cdot (-c \nabla w) = 0 \quad (2)$$

where  $w$  corresponds to the displacement along the  $x_3$  axis,  $\nabla = \left[ \frac{\partial}{\partial x}, \frac{\partial}{\partial y} \right]$  and where the

coefficients  $c$  and  $e_a$  are defined as follows:

$$c = \begin{bmatrix} C_{55} & 0 \\ 0 & C_{44} \end{bmatrix}; e_a = \rho, \quad (3)$$

in which  $\rho$  [ $\text{kg}/\text{m}^3$ ] is the mass density of the corresponding layer, having the corresponding elasticity matrix  $c$ . We used a boundary applied excitation, in accordance with the selected SH mode displacement field.

The equation is written for each layer of the assembly including the substrate/adhesive interphases and the continuity of displacements and stress between the layers is imposed. This 5-layer model (2 substrates, 1 adhesive layer and 2 interphases) is composed of layers of very different thicknesses. Such differences between thicknesses of different domains generates large variations in the size of the finite element mesh of the model. In order to avoid digital diffraction phenomena and to accurately describe wave propagation phenomena along the multi-layer, the size of the element must not suddenly change from one domain to another [27]. It is also necessary to ensure a sufficiently fine mesh size: in general, we consider at least 10 finite elements per wavelength. In the case of our waveguide, it was chosen to work with rectangular Lagrange elements, with a maximum size of  $\lambda_{\min} / 10 \approx 6.25\text{mm} / 10$  (with  $\lambda$  is the mode wavelength) in aluminium, glue and composite. In the case of the substrate/adhesive interphases, the element size is  $0.5 \mu\text{m}$ .

To simulate the propagation of a given mode, we apply the modal displacement in the cross section of the structure as obtained from a semi-analytical finite element method (SAFE - 1D model) [25], and this displacement will then be multiplied by a gaussian modulated harmonic function of time, in the following form:

$$f(t) = A \sin[2\pi f(t - t_0)] \exp\left[-\frac{t - t_c - t_0}{t_\varepsilon}\right]^2 \quad \text{for } t_0 < t < nT + t_0 \quad (4)$$

where  $A$  is the amplitude,  $t_0$  is the silence time before excitation (this time ensures the stability of the digital solution with less residual oscillations at the end of the structure),  $t_c$  is the time corresponding to the maximum of the signal,  $t_\varepsilon$  is a time related to the signal attenuation and  $nT$  corresponds to the excitation time. In this work, these parameters are defined as follow:

$$\left\{ \begin{array}{l} f = 360 \text{ kHz} \\ t_0 = 0.1 * T \quad \text{with } T = \frac{1}{f} \\ t_c = \frac{nT}{2} \quad \text{with } n = 4 \text{ cycles} \\ t_\varepsilon = \frac{t_c}{2} \end{array} \right. \quad (5)$$

The product of the displacement field 1D and the function  $f(t)$ , denoted M in Fig. 1 will be applied to the section on the left side of the guide. This mode propagates in the direction of propagation (along  $x_1$ -axis) over the entire length of the structure, i.e. 10 cm.

### 3.1.2 Modelling of a kissing bond defect at the substrate/adhesive interface

A literature review indicates a need for a clear and universally accepted definition of kissing bond defect. Based on contributions from several reputable industry sources and existing research in this area [28–31], the following definition of a kissing bond has been adopted for this work: kissing bond defect is considered as a contact without adhesion and is therefore modelled as a layer of air, without mass, characterized by its elastic constant  $C_{KB} = 10^5 \text{ Pa}$ .

A three-layer is modelled, with one area corresponding to perfect adhesion, and the interphase of the second area is replaced by the elastic constant of air to simulate the kissing bond. The length of each area is represented by the half distance of the total length of the guide (see Fig. 2). Once the model is solved, the time depending shear displacements of each substrate are collected for signal processing.

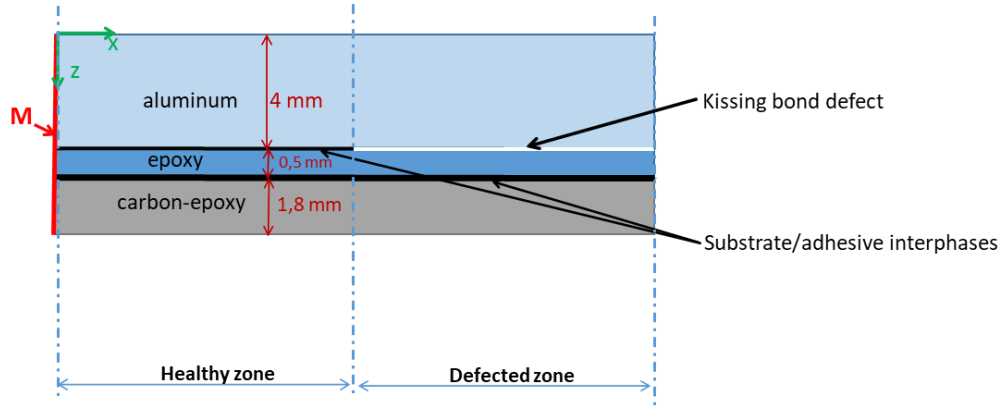


**Fig. 2.** Three-layer geometry with a degraded area.

### 3.1.3 Mode amplitude analysis by sliding window spatial FFT

#### *a. Signal processing*

This study focuses on the propagation of the  $SH_3$  mode at  $f = 630 \text{ kHz}$  because this mode was easily excited experimentally in the studied structures. This mode was chosen to have multiple wavelengths in the cross-section of the structure which should give better information on the quality of the coupling between the layers: its relatively high frequency range therefore makes it more sensitive to bonding quality defects. To our knowledge, mostly lower order modes have been studied so far for this type of characterisation [20–22]. Moreover, we have only succeeded in experimentally exciting the so-called insensitive wavenumber-frequency modes, in particular the  $SH_3$  mode (the criterion for selecting modes according to their sensitivity to bond quality is detailed in [8] and [25]). An insensitive wavenumber-frequency mode is a mode whose wavenumber at a given frequency is not modified by a property change (in our case a change in adhesive or cohesive properties): only the amplitude of this mode is modified from one sample to another.

In this model, the material viscosity is not considered, so no attenuation will be observed during the propagation in a given zone. A variation of the amplitude during the transition from

one zone to another should be indicative of a change in interface conditions. For this purpose, a spatial FFT with sliding window treatment at a selected frequency (here  $f = 630 \text{ kHz}$ ) is performed in order to follow the mode propagation in the structure: a temporal FFT is applied on the collected data, followed by a spatial FFT with a sliding window. The window used is rectangular with a size of 50 data points, i.e. about 4 wavelengths. A compromise is to be done between the size of the sliding window and the accuracy on the wavenumber values. The window is then completed by "zero-padding" up to  $2^{14}$  points giving a wavenumber step  $dk = 0.8 \text{ m}^{-1}$  which is a sufficient resolution, the averaged wavenumber values are around  $1000 \text{ m}^{-1}$ . The amplitude is deduced from the spatial FFT modulus plot as a function of position along the wave propagation in the structure. The modulus of the spatial FFT is affected to the centre of the sliding window. Consequently, the spatial representation is truncated at the beginning and at the end of the structure, by a distance equal to half of the sliding window size.

#### *b. Simulation results*

Fig. 3a shows in colour levels the amplitude of the  $\text{SH}_3$  mode at 300 kHz as a function of the position. In the perfect bonded zone between 0 and 5 cm, we can see the propagation of the  $\text{SH}_3$  mode without attenuation with a wavenumber of  $1000 \text{ m}^{-1}$  (see Fig. 3b). In the degraded zone (presence of the kissing bond between 5 and 10 cm), an increase of its amplitude, in the order of 20%, and an oscillatory behaviour is observed. It is possible to interpret the larger amplitude of the  $\text{SH}_3$  wave in the degraded area by a concentration of the acoustic energy on a smaller volume (that of the aluminium layer), as there is no longer any coupling between this layer and the adhesive-composite bilayer.

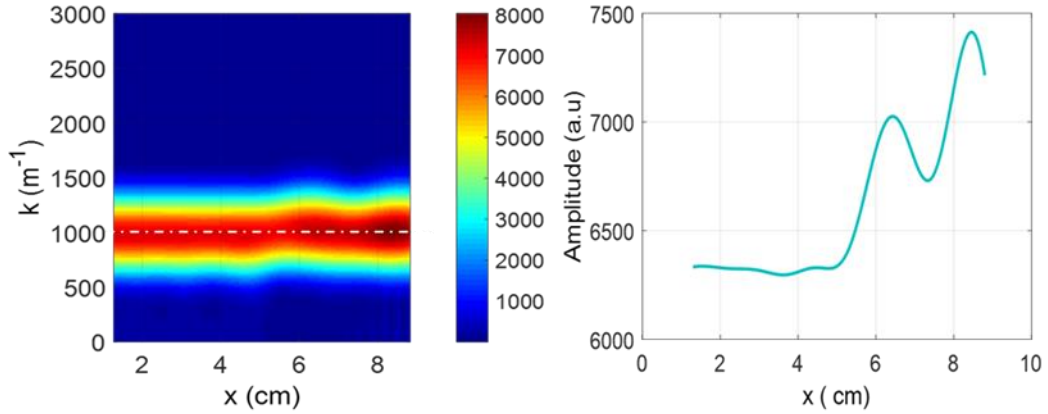


Fig. 3a

Fig. 3b

**Fig. 3 (a)** Evolution of the amplitude of the SH<sub>3</sub> mode at  $f = 630 \text{ kHz}$  in the three-layer structure with a degraded area - Displacements on the aluminium surface. The amplitude is in arbitrary unit. **(b)** Evolution of the amplitude of the SH<sub>3</sub> mode at  $k = 1000 \text{ m}^{-1}$  (numerical simulation).

The same signal processing is performed on the composite surface: as can be seen in Fig. 4.

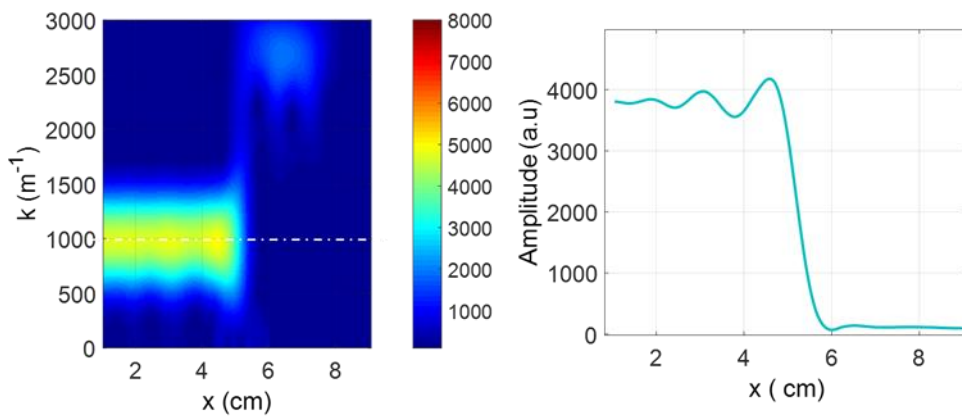


Fig. 4a

Fig. 4b

**Fig. 4 (a)** Evolution of the amplitude of the SH<sub>3</sub> mode at  $f = 630 \text{ kHz}$  in the three-layer structure with a degraded area - Displacements on the composite surface. The amplitude is in

arbitrary unit. **(b)** Evolution of the amplitude of the SH<sub>3</sub> mode at  $k=1000 \text{ m}^{-1}$  (numerical simulation).

The SH<sub>3</sub> mode amplitude becomes nearly null over the part with defect, which means that the energy transmission in the composite/epoxy bilayer is nearly zero and that most of the energy was transmitted in the aluminium single layer.

To confirm and to identify the modes propagating on the aluminium surface and on the composite surface in the degraded area, a 2D-FFT is performed to obtain the numerical dispersion curve in colour levels in the wavenumber-frequency domain (see Fig. 5). These results are superimposed on the three-layer dispersion curves in the case of a perfect adhesion in pink, the aluminium monolayer in green and the composite/epoxy bilayer in blue. The dispersion curves were obtained using the Semi-Analytical-FEM (SAFE) method, validated in previous works e.g. [15] and [17].

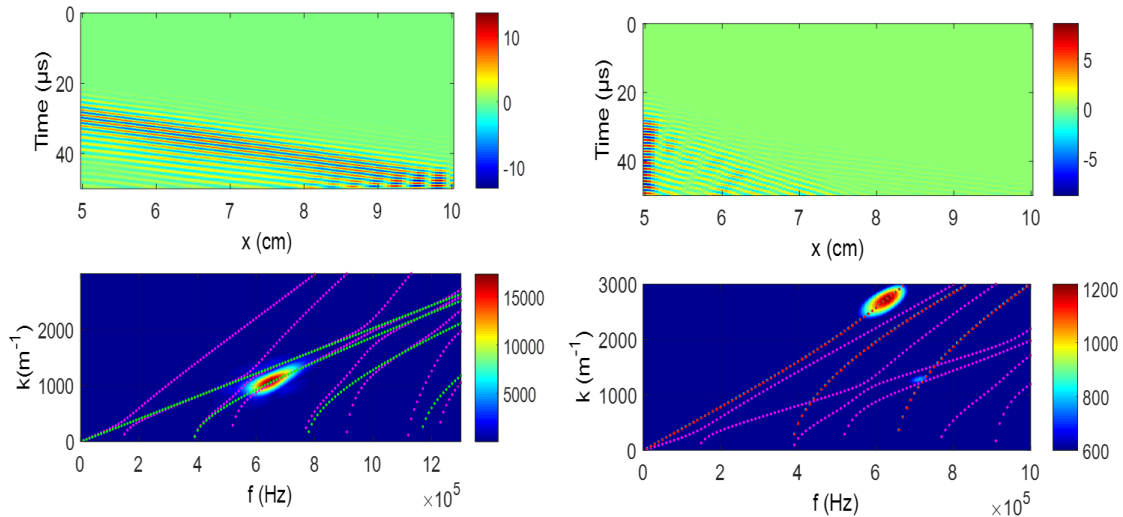


Fig. 5a

Fig. 5b

**Fig. 5.** Result of the FFT-2D on the degraded area: displacements on the aluminium surface (Fig. 5a) and on the composite surface (Fig 5.b). Superimposition of the three-layer dispersion

curves in the case of a perfect adhesion in pink, the aluminium monolayer in green and the composite/epoxy bilayer in red (numerical simulation).

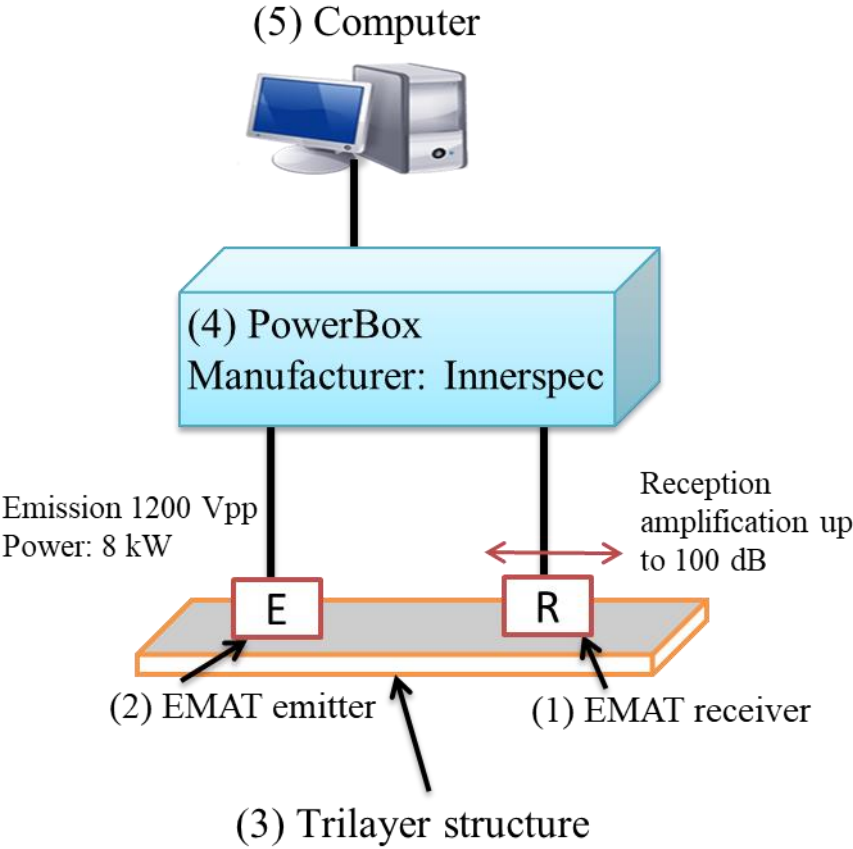
According to Fig. 5a, when the displacements are recovered on the aluminium surface (degraded zone), it is not possible to discriminate whether this mode is a three-layer mode or a monolayer mode. However, when the displacements are recovered on the composite surface (Fig. 5b), we clearly see a conversion from the  $SH_3$  mode of the three-layer to the  $SH_0$  mode of the composite/epoxy bilayer, indicating the total delamination between this composite/adhesive bilayer and the aluminium layer.

## **3.2 Experimental study**

### **3.2.1 Experimental setup and measurement method**

Fig. 6 shows the experimental setup composed of 2 EMAT (ElectroMagnetic Acoustic Transducers) and manufacturing by Innerspec (model: Powerbox 2). One of the advantages of this device is to generate ultrasonic waves without contact: it allows to avoid problems linked to coupling gel and thus ensures repetitive measurements of the displacement. A limitation of this particular device, due to its physical construction, is its inability to adequately work below a frequency of 150 kHz. Below this frequency, the mechanical resonances of the array cause a decreasing reverberation that obscures an increasingly important part of the omnidirectional near field [32]. Another limitation in using many EMATs is their usual limiting frequencies above the Megahertz [33], and therefore to achieve sub-millimetre resolution. EMATs are composed of a periodic arrangement of permanent magnets, producing a magnetic flux density with a period equal to the desired acoustic wavelength  $\lambda$ . An electric wire is placed between the magnets and the plate, and the current in the wire induces eddy currents in the metallic plate.

The interaction of the currents with the magnetic flux produces alternating Lorentz forces, normal to the direction of propagation, and parallel to the plate. This results in the generation of SH waves in the plate [34,35]. Waves will be generated on the aluminium side. Two transducers are used with the same wavelength  $\lambda = 6.25\text{ mm}$  : the emitter transducer enables to generate the SH<sub>3</sub> mode at  $f = 630\text{ kHz}$  . The excitation signal is amplitude modulated quasi-harmonic with a central frequency of 630 kHz and is composed of 10 cycles.



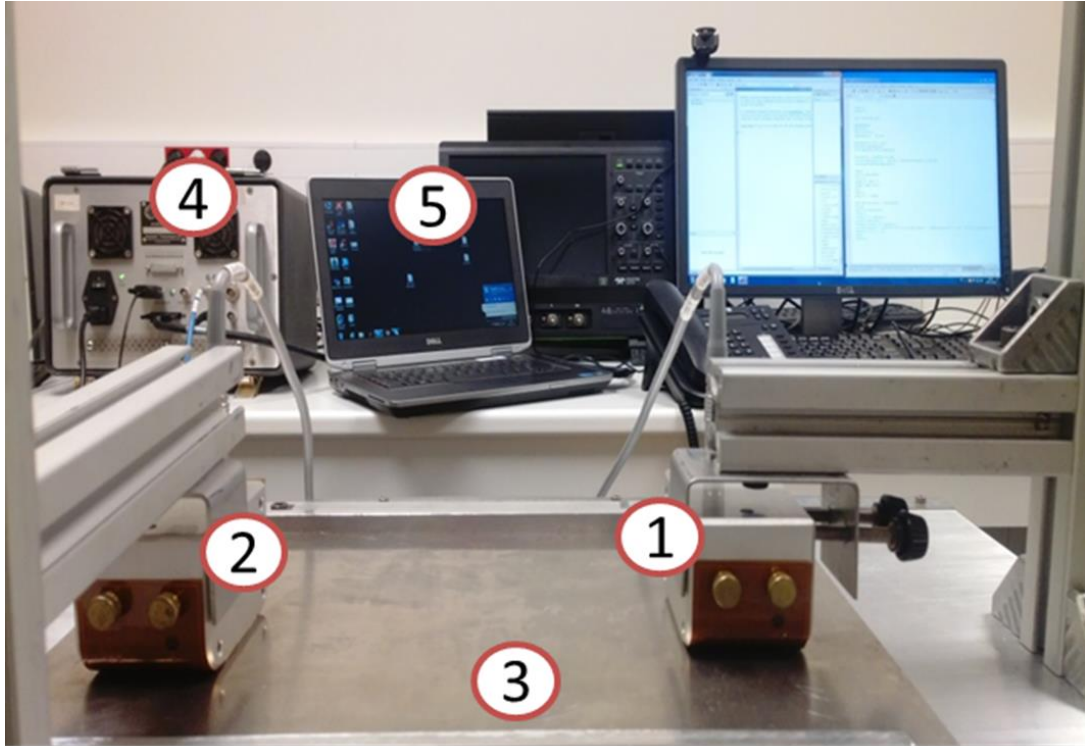


**Fig. 6.** Experimental setup.

The two transducers are placed face to face and initially at a distance of 1 cm from each other (this position corresponds to  $x = 0$ ). To ensure the same distance between the transmitter and the sample over the entire length of the study, the transducers are simply placed on the sample surface. To enhance the signal-to-noise ratio, the EMAT impedance is minimized by placing a capacitor in series in order to increase the current intensities, and the emitting signal is amplified up to 60 dB. Then the receiving transducer is translated in the direction of propagation on 6 cm distance with spatial steps of 61  $\mu\text{m}$ . For each position, the signal is acquired over a duration of 160  $\mu\text{s}$  corresponding to 8000 time samples, i.e. a sampling frequency of 50 MHz. The size of the time-position matrix is therefore 8000 rows and 983 columns. Fig. 7b. shows a plot of this matrix with time in ordinates, positions in abscissa and amplitude in colour levels, whereas Fig. 7a is the temporal signal for  $x=30$  mm: modes other than  $\text{SH}_3$  have been filtered out in Fig. 7.b.

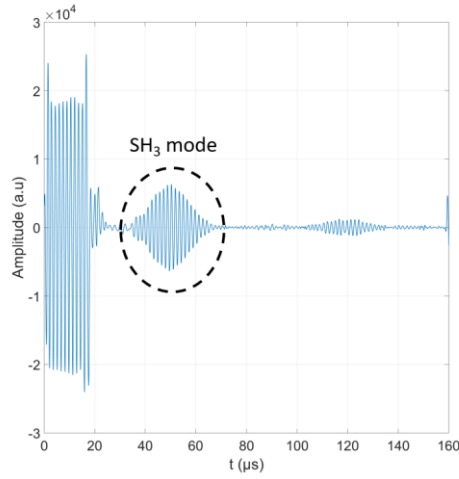


Fig. 7a

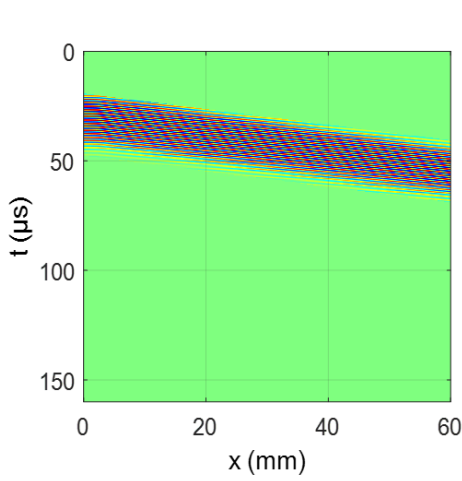


Fig. 7b

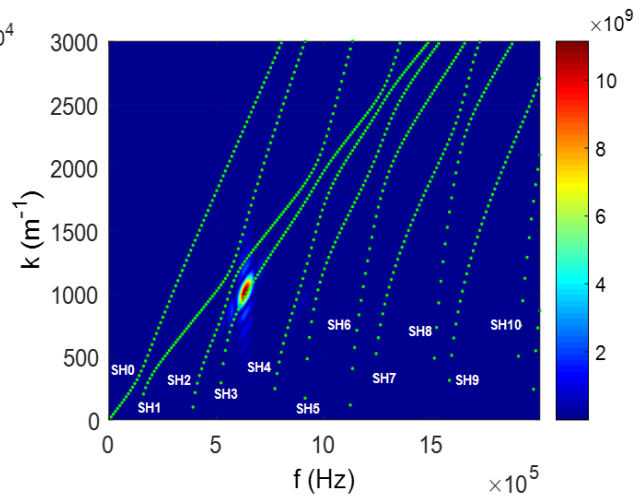
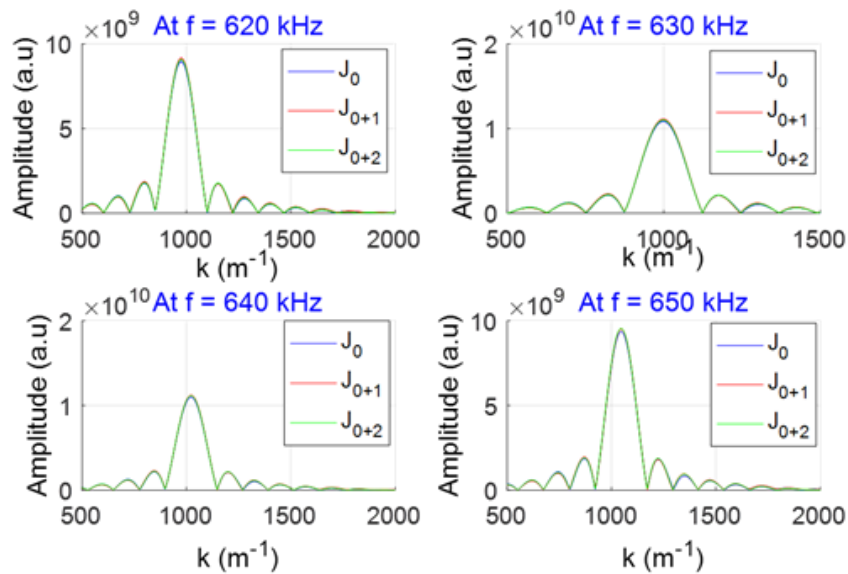


Fig. 7c

**Fig. 7** (a) Temporal signal for  $x=30$  mm. (b) Time-space representation of signal amplitudes measured by EMATs for the  $\text{Al}_{\text{DSi}}\text{E}_{100}\text{C}_{\text{N}}$  sample. The colour level is in arbitrary unit. (c) SH wave numerical dispersion curves for  $\alpha=\beta=1$  in green superimposed on the experimental curves for  $\text{Al}_{\text{DSi}}\text{E}_{100}\text{C}_{\text{N}}$  (experimental result).

### 3.2.2 Check of the reproducibility of measurements

The reproducibility study was done on the reference sample. For each sample, six identical experiments are conducted on different days in order to check the measurements reproducibility: the SH<sub>3</sub> mode is generated and its amplitude is acquired during its propagation. Fig. 8 shows an example of amplitude versus wavenumber record for the Al<sub>D</sub>SiE<sub>100</sub>C<sub>N</sub> sample, measured at Day 1, Day 2 and Day 3. The 3 curves are superimposed: this shows the good reproducibility in amplitude of the measurements. Indeed, the gap observed in amplitude is less than 1% from one experiment to another, regardless of the considered frequency.



**Fig. 8.** Reproducibility of SH<sub>3</sub> mode amplitude measurements at different frequencies for the Al<sub>D</sub>SiE<sub>100</sub>C<sub>N</sub> reference sample in different days D<sub>1</sub> ( $J_0$ ), D<sub>2</sub> ( $J_{0+1}$ ) and D<sub>3</sub> ( $J_{0+2}$ ) (experimental result).

### 3.2.3 Amplitude evolution of the SH<sub>3</sub> mode

Regarding the sample with the kissing bond defect ( $Al_{1/2DSi-1/2DRA}E_{100}C_N$  sample), we have plotted the evolution of the amplitude of the SH<sub>3</sub> mode in Fig. 9, by analogy with the study carried out in the numerical part (see section 3.1.3). From this figure, we can clearly distinguish the two zones due to the drastic change in amplitude when crossing from the zone without defect to the one with defect. A higher amplitude is indeed observed on the degraded area than on the area with good adhesion, which is in good agreement with the numerical results: the energy transmitted from the well bonded area to the degraded area will be concentrated on only one layer, that of aluminium, while it was distributed over the three layers constituting the assembly in the nondegraded area. The ratio of the amplitudes between the kissing bond zone and the high adhesion zone is 1.25 for the experimental results and 1.13 for the numerical results, which represents a difference of 10%. This result is satisfactory given the approximations of the model, in particular the non-accounting of the angular opening of the transducer and the viscosity of the materials.

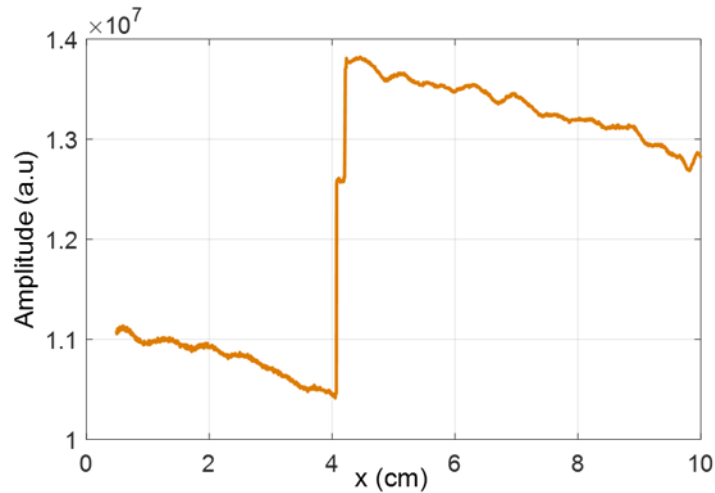


**Fig. 9.** Amplitude evolution of the SH<sub>3</sub> mode versus distance covered for

$Al_{1/2DSi-1/2DRA}E_{100}C_N$  sample (experimental result).

#### 4. Discrimination of adhesion levels by measuring mode attenuation

From the experimental protocol detailed in section 3.2, we can extract information on the amplitude of the propagated mode in the different samples. The aim is to discriminate between samples by propagating an insensitive SH mode in the frequency-wave domain and studying its attenuation during propagation, while having excited this mode under the same experimental conditions, and by applying an identical signal processing for all samples. Mode attenuation is deduced from the temporal FFT module (that gives the amplitude of the propagating wave) plot of each time signal at the different positions. Fig. 10 shows the attenuation profile of SH<sub>3</sub> mode in  $Al_{DSi}E_{100}C_N$  and  $Al_DE_{80}C_N$  samples as a function of the scanned distance.

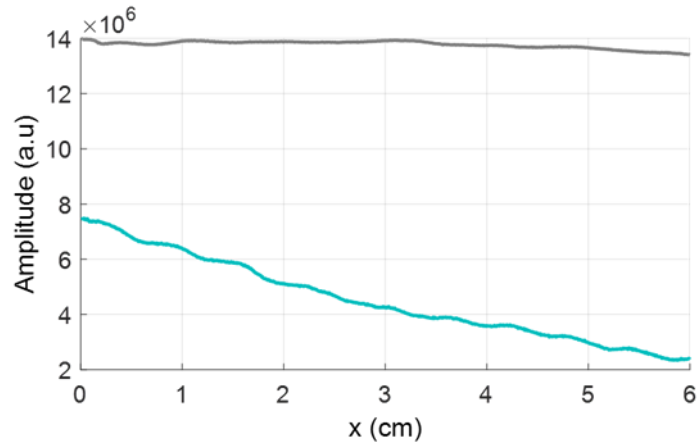


**Fig. 10.** Evolution of SH<sub>3</sub> mode at  $f = 630 \text{ kHz}$  attenuation versus distance covered for  $Al_{DSi}E_{100}C_N$  in grey and for  $Al_DE_{80}C_N$  in blue (experimental result).

The logarithm of the amplitude is then plotted versus position and a linear fit is applied. The attenuation coefficient  $k''$  of the propagating mode is then deduced from the slope of this linear fit, and are collected on Table 4. It should be recalled that the  $Al_{DSi}E_{100}C_N$  sample has a priori a

nominal adhesion level and that the  $Al_D E_{80} C_N$  sample has a lower adhesion. One can see that the attenuation in the sample with high adhesion level is lower than in the sample with weak adhesion level. Another way to discriminate the samples, and thanks to the reproducibility of the experiments with EMAT transducers, is to compare the amplitude of the generated wave at the first receiver position, following the criterion: the amplitude of the generated wave should increase with the quality of the bonding. In Fig. 10, it is indeed noted that the initial amplitude associated with the  $Al_{DSi} E_{100} C_N$  sample is significantly higher than the amplitude of the  $Al_D E_{80} C_N$  sample, so the mode is better propagated than for a lower level of adhesion. Table 4 reports the calculated attenuation coefficient and the amplitude at the initial position for these two samples. It can also be seen that the attenuation of the SH<sub>3</sub> mode is higher for the  $Al_D E_{80} C_N$  sample than for the  $Al_{DSi} E_{100} C_N$  one. This result highlights the effectiveness of chemical treatment with silane to promote optimal energy transmission through the three layers of the guide and thus improve the coupling between the substrate and the adhesive.

Samples	k'' attenuation coefficient of SH <sub>3</sub> mode (m <sup>-1</sup> )	Amplitude at the initial position (a.u.)
$Al_{DSi} E_{100} C_N$	0.45	$14 \cdot 10^6$
$Al_D E_{80} C_N$	17	$7.14 \cdot 10^6$

**Table 4.** Attenuation coefficient and amplitude at the initial position for  $Al_{DSi} E_{100} C_N$  and

$Al_D E_{80} C_N$  samples.

From the results in the (k,f) plane, a cut at f=630 kHz for samples  $Al_{DSi} E_{100} C_N$  and  $Al_D E_{80} C_N$  is plotted in Fig. 11 proves that the SH<sub>3</sub> mode has a wavenumber which is quasi-independent of the bonding quality at the studied frequencies. Its wave number is almost the same for both

samples, so that the wavenumber is not a discriminating factor capable to distinguish the adhesion levels. On the other hand, the amplitude of the mode is much more important for the sample with a high level of adhesion, as seen in Fig. 10. Studies [36,37] have shown that there is a link between attenuation and resonance width: the resonance width is indicator on the attenuation of the propagating wave. We therefore define a coefficient  $\chi$  as follows:

$$\chi = \frac{\Delta k_{\frac{A_{\max}}{2}}}{A_{\max}}$$

where  $\Delta k_{\frac{A_{\max}}{2}}$  is the width at half height in wavenumber and  $A_{\max}$  is the maximum amplitude.

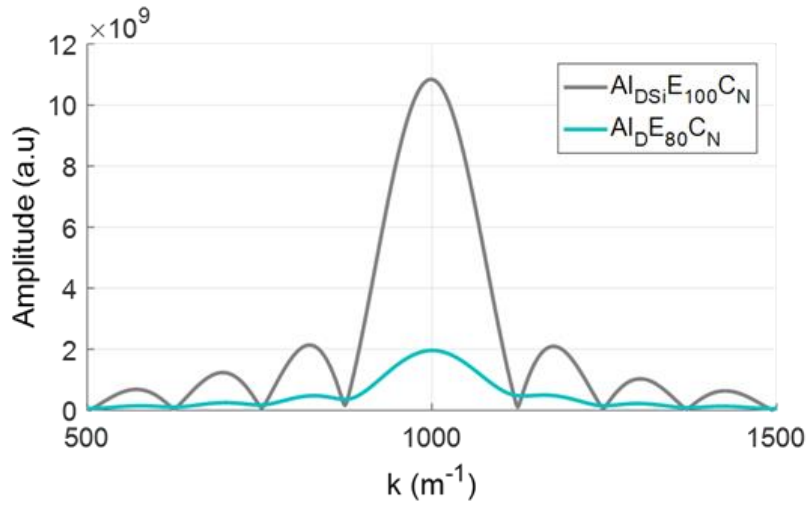


**Fig. 11.** Amplitude comparison of SH<sub>3</sub> mode at  $f = 630\text{kHz}$  for  $Al_{DSi}E_{100}C_N$  in grey and for

$Al_{DE80}C_N Al$  in blue (experimental result).

These two quantities varying in opposite directions, the larger  $\chi$  is, the higher the attenuation would be. This coefficient is calculated for both samples and compared to the attenuation  $k''$  (see Table 5). It can be observed that the evolution of  $k''$  follows the same trend as that of  $\chi$  for

both samples. We can conclude that the better the bonding quality is, the lower are the attenuation and consequently the ratio  $\chi$ .

Samples	$\Delta k_{A_{\max}/2}$ en ( $\text{m}^{-1}$ )	$A_{\max}$ (u.a)	$\chi$ ( $10^{-8} \text{m}^{-1}$ )	$k''$ ( $\text{m}^{-1}$ )
$Al_{DSi}E_{100}C_N$	149	$1.08 \cdot 10^{10}$	1.38	0.45
$Al_D E_{80} C_N$	158	$1.96 \cdot 10^9$	8.06	17.00

**Table 5.** Values of the resonance width ( $\chi$ ) and the attenuation coefficient ( $k''$ ) for the

$Al_{DSi}E_{100}C_N$  and  $Al_D E_{80} C_N$  samples.

## 5. Conclusions

In this work, results are given on using the SH3 mode to indicate the level of adhesion and to detect the presence a kissing bond type defect in a three-layer, based on the analysis of the amplitude variation of the SH wave.

A numerical 2D model was presented, capable to predict the signature of the presence of a kissing bond, that is a delamination of the three-layer into one layer where high transmission occurs, and one bilayer where zero transmission is observed. The experiments were conducted with EMAT transducers which allow a high reproducibility of the measurements. Experiments and numerical results are in good agreement.

To discriminate adhesion levels, the analysis of the amplitude versus position gives 4 parameters to classify the adhesion level. The first parameter is the attenuation during the propagation, which is lower for the higher level of adhesion three-layer, which shows the strong coupling between the layers. The second parameter is the excitation amplitude of the wave: the

stronger the coupling, the higher the amplitude. The third parameter is based on the well-known link between the resonance width of the wave, and its attenuation: the larger the width, the more attenuating the medium. The fourth parameter which is the ratio between the last two parameters was defined to enhance their effects, proving to be a good indicator of the bonding quality.

This study was possible due to the amplitude reproducibility of the EMATs, which has been experimentally validated. Many work perspectives could constitute an interesting continuation of this research: from an acoustic characterization point of view, one could test many more samples, especially industrial samples, by reducing the size of the kissing bond defect down to the wavelength, to confirm and generalize the results found in this work. This would make it possible to establish a database that can be used to characterise similar assemblies. From a numerical modelling point of view, the development of a 3D model could be envisaged. Indeed, the 3D modelling would make it possible to consider the angular aperture of the transducer beam. It would thus be better adapted to reproduce more accurately the experimental conditions. Improved comparisons could then be made between the measurements and the simulation.

## **Acknowledgements**

This research work has been financially supported by Le Havre Seine Métropole (LHSM), the Normandy Region and the European Regional Development Fund via the RIN DIADEMAR and the INTERREG TIGER projects.

## **References**

- [1] Adams RD, editor. Adhesive Bonding. Woodhead Publishing; 2005.  
<https://doi.org/10.1533/9781845690755.3.frontmatter>.

- [2] Ishii Y, Biwa S. Evaluation of interlayer interfacial stiffness and layer wave velocity of multilayered structures by ultrasonic spectroscopy. *The Journal of the Acoustical Society of America* 2014;136:183–91. <https://doi.org/10.1121/1.4881920>.
- [3] Benyahia F, Albedah A, Bouiadjra BB. Analysis of the adhesive damage for different patch shapes in bonded composite repair of aircraft structures. *Materials & Design (1980-2015)* 2014;54:18–24. <https://doi.org/10.1016/j.matdes.2013.08.024>.
- [4] Benyahia F, Bouanani MF, Albedah A, Bouiadjra BB, Achour T. Effect of water absorption on the adhesive damage in bonded composite repair of aircraft structures. *Materials & Design* 2014;57:435–41. <https://doi.org/10.1016/j.matdes.2013.12.081>.
- [5] Pantelakis Sp, Tserpes KI. Adhesive bonding of composite aircraft structures: Challenges and recent developments. *Science China Physics, Mechanics and Astronomy* 2014;57:2–11. <https://doi.org/10.1007/s11433-013-5274-3>.
- [6] Su Z, Ye L, Lu Y. Guided Lamb waves for identification of damage in composite structures: A review. *Journal of Sound and Vibration* 2006;295:753–80. <https://doi.org/10.1016/j.jsv.2006.01.020>.
- [7] Castaings M, Hosten B. Guided waves propagating in sandwich structures made of anisotropic, viscoelastic, composite materials. *The Journal of the Acoustical Society of America* 2003;113:2622–34. <https://doi.org/10.1121/1.1562913>.
- [8] Leduc D, El-Kettani ME-C, Attar L, Predoi MV, Pareige P. Bonding Characterization of a Three-Layer Metal-Adhesive-Metal Using Shear Horizontal Modes of Close Dispersion Curves. *Acta Acustica United with Acustica* 2017;103:926–31. <https://doi.org/10.3813/aaa.919121>.
- [9] Predoi MV, Attar L, El Kettani E-CM, Leduc D, Pareige P. Analysis of Shear Waves in Bonded Layers Using Springs Model. *Romanian Journal of Acoustics and Vibration* 2019.
- [10] Ismaili NA, da Silva CDM, El-Kettani ME-C, Despau G, Rousseau M, Izbicki J-L. Lamb Modes for the Characterization of Bonded Structures. *Acta Acustica United with Acustica* 2013;99:331–4. <https://doi.org/doi:10.3813/AAA.918615>.
- [11] Lowe MJS, Challis RE, Chan CW. The transmission of Lamb waves across adhesively bonded lap joints. *The Journal of the Acoustical Society of America* 2000;107:1333–45. <https://doi.org/10.1121/1.428420>.
- [12] Heller K, Jacobs LJ, Qu J. Characterization of adhesive bond properties using Lamb waves. *NDT & E International* 2000;33:555–63. [https://doi.org/10.1016/S0963-8695\(00\)00022-0](https://doi.org/10.1016/S0963-8695(00)00022-0).
- [13] Rokhlin SI. Lamb wave interaction with lap-shear adhesive joints: Theory and experiment. *The Journal of the Acoustical Society of America* 1991;89:2758–65. <https://doi.org/10.1121/1.400715>.
- [14] Hirao M, Ogi H. An SH-wave EMAT technique for gas pipeline inspection. *Ndt & E International* 1999;32:127–32.
- [15] Predoi MV, Ech Cherif El Kettani M, Leduc D, Pareige P, Coné K. Use of shear horizontal waves to distinguish adhesive thickness variation from reduction in bonding strength. *The Journal of the Acoustical Society of America* 2015;138:1206–13. <https://doi.org/10.1121/1.4928299>.
- [16] Flynn P. Cohesive bond strength prediction for adhesive joints. *Journal of Testing and Evaluation* 1979;7:168–71.
- [17] Gauthier C, Ech-Cherif El-Kettani M, Galy J, Predoi M, Leduc D, Izbicki J-L. Lamb waves characterization of adhesion levels in aluminum/epoxy bi-layers with different cohesive and adhesive properties. *International Journal of Adhesion and Adhesives* 2017;74:15–20.

- [18] Gauthier C, Galy J, El-Kettani ME-C, Leduc D, Izbicki J-L. Evaluation of epoxy crosslinking using ultrasonic Lamb waves. *International Journal of Adhesion and Adhesives* 2018;80:1–6. <https://doi.org/10.1016/j.ijadhadh.2017.09.008>.
- [19] Gauthier C, Ech-Cherif El-Kettani M, Galy J, Predoi M, Leduc D. Structural adhesive bonding characterization using guided Lamb waves and the vertical modes. *International Journal of Adhesion and Adhesives* 2020;98:102467. <https://doi.org/10.1016/j.ijadhadh.2019.102467>.
- [20] Koodalil D, Barnoncel D, Rajagopal P, Balasubramaniam K. Interfacial adhesion (kissing bond) detection using shear horizontal (SH) waves. *AIP Conference Proceedings* 2019;2102:020042. <https://doi.org/10.1063/1.5099746>.
- [21] Koodalil D, Barnoncel D, Rajagopal P, Balasubramaniam K. Detection of interfacial weakness in a lap-shear joint using shear horizontal guided waves. *NDT & E International* 2020;112:102248. <https://doi.org/10.1016/j.ndteint.2020.102248>.
- [22] Arun K, Dhayalan R, Balasubramaniam K, Maxfield B, Peres P, Barnoncel D. An EMAT-based shear horizontal (SH) wave technique for adhesive bond inspection. *AIP Conference Proceedings* 2012;1430:1268–75. <https://doi.org/10.1063/1.4716364>.
- [23] Koodalil D, Rajagopal P, Balasubramaniam K. Quantifying adhesive thickness and adhesion parameters using higher-order SH guided waves. *Ultrasonics* 2021;114:106429. <https://doi.org/10.1016/j.ultras.2021.106429>.
- [24] Multiphysics C. Introduction to COMSOL multiphysics®. COMSOL Multiphysics, Burlington, MA, Accessed Feb 1998;9:2018.
- [25] Attar L, Leduc D, El Kettani MEC, Predoi MV, Galy J, Pareige P. Detection of the degraded interface in dissymmetrical glued structures using Lamb waves. *NDT & E International* 2020;111:102213.
- [26] Mittal KL. Adhesion measurement of thin films, thick films and bulk coatings. *Am Soc Test Mat*; 1978.
- [27] Drozd M, Skelton E, Craster RV, Lowe MJS. Modeling Bulk and Guided Waves in Unbounded Elastic Media Using Absorbing Layers in Commercial Finite Element Packages. *AIP Conference Proceedings* 2007;894:87–94. <https://doi.org/10.1063/1.2717958>.
- [28] Kundu T, Maji A, Ghosh T, Maslov KI. Detection of kissing bonds by Lamb waves. *Ultrasonics* 1998;35:573–80.
- [29] Yan D, Drinkwater BW, Neild SA. Measurement of the ultrasonic nonlinearity of kissing bonds in adhesive joints. *NDT & E International* 2009;42:459–66. <https://doi.org/10.1016/j.ndteint.2009.02.002>.
- [30] Nagy PB. Ultrasonic classification of imperfect interfaces. *Journal of Nondestructive Evaluation* 1992;11:127–39. <https://doi.org/10.1007/BF00566404>.
- [31] Adams DE, Sharp ND, Myrent N, Sterkenburg R. Inspection for kissing bonds in composite materials using vibration measurements. In: Wu HF, editor. *Nondestructive Characterization for Composite Materials, Aerospace Engineering, Civil Infrastructure, and Homeland Security* 2011, vol. 7983, SPIE; 2011, p. 268–75. <https://doi.org/10.1117/12.878680>.
- [32] Wilcox P, Lowe M, Cawley P. Omnidirectional guided wave inspection of large metallic plate structures using an EMAT array. *IEEE Trans Ultrason Ferroelectr Freq Control* 2005;52:653–65. <https://doi.org/10.1109/tuffc.2005.1428048>.
- [33] Murray PR, Dewhurst RJ. Application of a laser/EMAT system for using shear and LS mode converted waves. *Ultrasonics* 2002;40:771–6. [https://doi.org/10.1016/S0041-624X\(02\)00213-5](https://doi.org/10.1016/S0041-624X(02)00213-5).
- [34] Bernstein JR, Spicer JB. Hybrid laser/broadband EMAT ultrasonic system for characterizing cracks in metals. *J Acoust Soc Am* 2002;111:1685–91.

- [35] Ribichini R, Cegla F, Nagy PB, Cawley P. Study and comparison of different EMAT configurations for SH wave inspection. *IEEE Trans Ultrason Ferroelectr Freq Control* 2011;58:2571–81. <https://doi.org/10.1109/TUFFC.2011.2120>.
- [36] Uberall H. *Acoustic Resonance Scattering*. CRC Press. 1992.
- [37] Fiorito RB, Madigosky WM, Überall H. Resonance theory of acoustic waves interacting with an elastic plate. *Journal of the Acoustical Society of America* 1979;66:1857–66.